



# pH-dependent channel gating in connexin26 hemichannels involves conformational changes in N-terminus

Xia Wang<sup>a,b</sup>, Xue Xu<sup>a,b</sup>, Ming Ma<sup>a,b</sup>, Wei Zhou<sup>a,b</sup>, Yonghua Wang<sup>a,b,\*</sup>, Ling Yang<sup>c</sup>

<sup>a</sup> Center of Bioinformatics, Northwest A&F University, Yangling, Shaanxi, 712100, China

<sup>b</sup> College of Life Sciences, Northwest A&F University, Yangling, Shaanxi, 712100, China

<sup>c</sup> Lab of Pharmaceutical Resource Discovery, Dalian Institute of Chemical Physics, Chinese Academy of Sciences, Dalian, Liaoning, 116023, China

## ARTICLE INFO

### Article history:

Received 19 August 2011

Received in revised form 23 December 2011

Accepted 27 December 2011

Available online 5 January 2012

### Keywords:

Molecular dynamic simulation

Connexin26

pH

Channel gating

## ABSTRACT

Connexin (Cx) hemichannels controlling an exchange of ions and metabolites between the cytoplasm and extracellular milieu can be modulated by the variation of intracellular pH during physiological and pathological conditions. To address the mechanism by which the pH exerts its effect on hemichannels, we have performed two 100-ns molecular dynamics simulations of the Cx26 channel in both acidic and neutral states. The results show that: 1) transmembrane domains undergo clockwise motions around the pore axis under both acidic and neutral conditions, while extracellular segments keep stable. 2) Under neutral condition, Cx26 has a tightly closed configuration that occurs through the assembly of N-terminal helix (NTH) region. This shows a constriction formed by the interhelical interactions of Asp2 and Met1 from neighboring NTH, which shapes the narrowest segment (pore radius < 2 Å) of the pore, preventing the passage of ions from the extracellular side. This indicates that Asp2 may act as a channel gate. 3) Under the acidic condition, the constriction is relieved by the protonation of Asp2 causing interruption of interhelical interactions, Cx26 has a flexibly opening pore (pore radius > 4.5 Å) around NTH region, allowing the passage of chloride ions unimpeded by the side-chain Asp2. While in the extracellular part two chloride ions interact with the side-chain Lys41 from three subunits. Finally, we provide a plausible mechanism of pH-dependent gating of hemichannel that involves protonation of the aspartic residues, suggesting that the pH sensitivity of hemichannel permeability is a sophisticated mechanism for cell regulating ion permeation.

© 2011 Elsevier B.V. All rights reserved.

## 1. Introduction

Intracellular pH ( $pH_i$ ) varies under different physiological and pathological conditions. Modest fluctuations in  $pH_i$  can arise during physiological cellular activity such as changes of neuronal activity or the resting potential [1], and larger fluctuations occur under pathological conditions such as hypoxia, or ischemia [2,3]. In recent decades, the variation of pH values has been regarded as a fundamental determinant of intercellular electrical and metabolic communication mediated by gap junctions (GJs) and paracrine signaling through nonjunctional/unopposed hemichannels [4].

GJs are ubiquitous membrane components of higher organisms that allow the ions and small molecules under ~1.0 kilodaltons (kDa) to be transferred between the cytoplasm of adjacent cells and thus greatly influence homeostasis, development and other cellular processes (for comprehensive reviews, see [5,6]). Each GJ channel is formed by the end-to-end non-covalent docking of two hemichannels, also known as connexons [7], each composed of six connexin

protomers and supplied by one of the two adjacent cells. At present, more than 20 types of connexins have been identified in mammals [8], which are commonly designated with numerical suffixes referring to the molecular weight of the deduced sequence in kDa (e.g., connexin26 or Cx26 has a mass of 26 kDa) [9].

On the molecular scale, substantial efforts have been devoted to understanding the mechanical properties of pH-dependent modulation of hemichannels [10–12]. The crystal structure of the gap junction channel has shown a donut like structure, which is comprised of [9] an N-terminal helix (NTH), four transmembrane (TM) segments (designated TM1 to TM4), and two extracellular loops (E1 and E2) as well as a variable portion consisting of the cytoplasmic loop (CL) (Fig. 1). Several domains in the CL and carboxy terminal (CT) domains of Cx43 seem to be involved in pH-dependent gating [10–12]. Especially, mutations of His residues in the CL of this protein significantly affect pH sensitivity, suggesting that protonation of these residues may be important in the pH-dependent GJs [13]. In Cx32, charge interactions within CL, as well as between CL and the proximal portion of CT, have been suggested to be responsible for pH sensitivity [14]. The pH-dependent interaction between the gap junction and the other cytoplasmic proteins may play an important role in the remodeling of gap junctions and in protection from lesion spread

\* Corresponding author at: Center of Bioinformatics, Northwest A&F University, Yangling, Shaanxi, 712100, China. Tel.: +86 29 87092262.

E-mail address: [yh\\_wang@nwsuaf.edu.cn](mailto:yh_wang@nwsuaf.edu.cn) (Y. Wang).

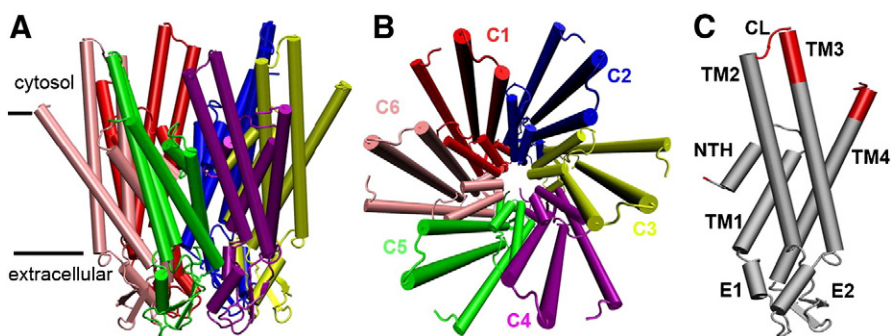


**Fig. 1.** Overall structure of the Cx26 hemichannel in cartoon representation. The corresponding protomers (connexins) in the hemichannel are shown in the different colors. (A) View of the Cx26 hemichannel as would be seen along the plane of the lipid bilayer, oriented such that the upper side represents the intracellular half. (B) Top view of the Cx26 hemichannel showing the arrangement of the transmembrane helices TM1 to TM4. (C) Side view of the Cx26 protomer in cartoon representation. E1 and E2 are the loops connecting TM1 and TM2, and TM3 and TM4, respectively. Cytoplasmic loop (CL) is the loop linking TM2 and TM3. The reconstructed residues are highlighted in red.

after local ischemic injury [15]. Although multiple domains of the connexin polypeptides contribute to the biophysical properties of gap junction channels and hemichannels, several of the amino acids within the NT have important roles in voltage-dependent gating, unitary conductance, and permeability (reviewed by [16]). The NT segment of the structure possesses sixfold rotational symmetry, with the channel pore is very constricted near Asp2 which probably serves as plugs blocking the channel [9]. This structure suggests that physical blockage by a plug is an essential part of a gating mechanism and is consistent with the physiological studies that each connexon can regulate its activity autonomously [17,18]. This concept is supported by recent electron microscopy studies that showed a prominent density in the center of the pore in Cx26 [19], which was decreased in the N-terminal deletion mutant Cx26 (Met34Ala-del2-7) [20]. Furthermore, many mutations identified in all domains of the connexin polypeptide, particularly in the NT region (residues 1 to 22) of connexins, have been associated with a variety of inherited pathologies including sensorineural deafness (non-syndromic and syndromic, especially associated with skin diseases), X-linked Charcot–Marie–Tooth disease, cataracts, oculodentodigital dysplasia, and keratodermas (reviewed in [16]).

Several particularly interesting questions arise from these strong cell biological, biochemical, and biophysical evidences: What are the mechanisms of pH modulation on GJs? What conformational changes in connexons will occur, thus facilitating ions or metabolites transfer from one cell to another, and regulating intracellular signaling? To address these, one needs first to understand the molecular basis of channel gating by identifying connexin domains relevant to gating, evaluating the likely participation of accessory molecules, and probing gating by pharmacological, genetic and theoretical tools. Since the molecular mechanisms that underlie this modulation of connexin channel activity may differ among connexin isoforms, here, we characterize pH-dependent modulation of Cx26, the second-smallest member of the conserved mammalian gap junction protein family, by performing a 100-ns all-atom molecular dynamics (MD) simulation of the Cx26 in an explicit solvent-membrane context at neutral pH (pH = 7). In parallel, we also examine the protein in a lower pH value (pH = 4), by setting the charges of the ionizable residues of the channel to their standard state at acidic pH. The results suggest that the channel can switch between two distinct states of its N-terminal segment with either open ends in acidic pH or closed ends in neutral pH, a process that forms the basis for cellular protection.

## 2. Results and discussion

Recently, several MD simulations of large membrane proteins including the rhodopsin (~43,000 atoms) [21], the  $\beta$ 2-adrenergic receptor (~99,000 atoms) [22], the integral Kv1.2 ion channel

(~120,000 atoms) [23] and the *Gloeobacter violaceus* receptor (~200,000 atoms) [24] have been carried out. Here, much larger systems of the fully hydrated membrane-inserted hemichannel Cx26 comprising ~300,000 atoms in both neutral and acidic pHs have been simulated for 100 ns, respectively.

### 2.1. Dynamics of the hemichannel in both neutral and acidic states

The overall drift of Cx26 from the initial structure provides a measure of the conformational stability of this protein in a membrane environment. Drift can be simply characterized by the C $\alpha$  coordinate root mean square displacement (RMSD) relative to the starting (crystal) structure. In the course of the MD simulation performed on the Cx26 model in the neutral state, the RMSD of the whole connexon rapidly increases during the initial 20 ns of the simulation, and then stabilizes at ~4.4 Å (Fig. 2A). The final RMSD values for the TM region (Fig. 2A) range from 2 to 3.8 Å for individual connexins, indicative of a very stable behavior. The differences between the RMSDs calculated over the TM segments of the connexon and those of the separated connexins suggest that the structure of the helix bundles is still stable whereas the protein quaternary structure undergoes global rearrangement during the simulation time. For the acidic state, the steady-state RMSD of the whole connexon (TM segments) (~3.9 Å) is a little lower than the values observed in the neutral state, indicative of a relatively smaller global rearrangement of protein quaternary structure.

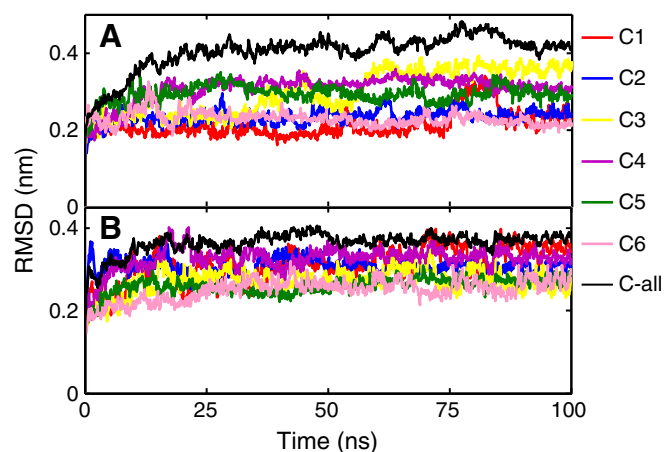


**Fig. 2.** Root mean square deviations (RMSDs) calculated over the C $\alpha$  atoms of all the TM domains of the connexon (black) and sole TM domain of the connexin. (A) and (B) represent the RMSDs of Cx26 in neutral and acidic pHs, respectively. C1 to C6 represent connexins 1 to 6, respectively.

Considering the conformational rearrangement of Cx26 in both acidic and neutral conditions, we are interested in further examination and comparison of the magnitude of the conformational fluctuations in different regions of the structure in two states. To guarantee that calculated parameters reflect the intrinsic properties of each system, the analyses of MD trajectories have been performed by discarding the first 30 ns for all simulations. The C $\alpha$  root mean square fluctuations (RMSFs) around the average structure of each protomer from the last 70 ns simulation are calculated. In Fig. 3B, the C $\alpha$  RMSFs are shown as a function of residue number for each protomer of Cx26, and compared with the equivalent RMSFs derived from the average B-factors. The residue RMSF values well reproduce the crystallographic B-factors. While the  $\alpha$ -helices and the  $\beta$ -strands have, in the simulations, significantly lower fluctuations than the equivalent RMSFs derived from the B-factors. This probably reflects some contribution of static crystal disorder (e.g., mosaicity) to the B-factors as well as undersampling of long-timescale motions of the channel [25]. Such an interpretation is supported by recent simulations of the small outer membrane protein OmpT in a crystal versus a bilayer environment [26].

The RMSF values show that all six protomers in each of both models exhibit virtually identical patterns, with the high fluctuations ( $\sim 5$  Å) being seen in the CL and C-terminal regions and the lowest fluctuations ( $\sim 1$  Å) in the transmembrane helices (NTH, TM1 to TM4). As the former is oriented away from the rest of the protein, toward the surrounding cytosol, they are expected to show the greatest mobility. In line, this region shows weak electron density in the crystal structure of Cx26, suggesting a substantial degree of flexibility [9]. The latter remains relatively invariant because they are stabilized by dipole–dipole interactions of the antiparallel helices (details in Section 2.2) and the intra-protomer interactions including three disulphide bonds (Cys53–Cys180, Cys60–Cys174, Cys64–Cys169) in the extracellular part of the transmembrane region. Notably, the regions located “behind” the NTH in the three-dimensional structure (Fig. 1C, the intramembrane part of the TM1 and TM2 of the six protomers) form the inner wall of the pore, showing remarkably stability ( $\sim 0.8$  Å) throughout the simulation in the neutral and acidic conditions. Compared with the TM1 and TM2, the NTHs (residues 1–11) have relative higher fluctuations ( $\sim 1.1$  Å), which are probably induced by the flexible loop ( $\sim 2$  Å) connecting the NTH to TM1 (Fig. 3), indicating that the NTHs are the relative mobile domains in the structure. This finding agrees with an NMR solution structure of an N-terminal peptide of Cx26,

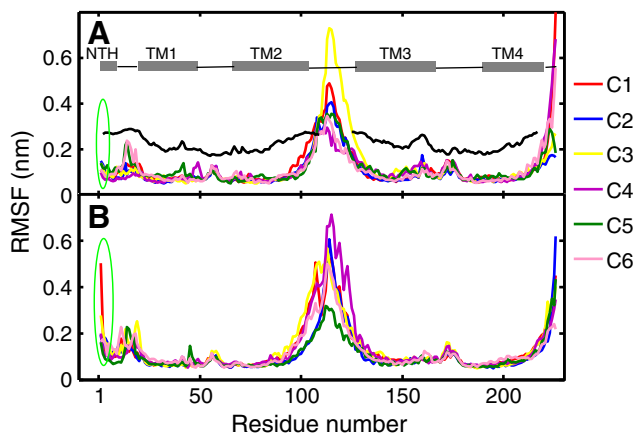


**Fig. 3.** Root-mean square fluctuation (RMSF) of C $\alpha$  atoms of Cx26, with each protomer displayed separately. (A) and (B) indicate the RMSF of Cx26 in neutral and acidic pH, respectively. C1 to C6 represent connexins 1 to 6, respectively. The black curve denotes the RMSF derived from the B-factor. The secondary structure regions of the protein are identified for clarity. The first three residues  $^1\text{Met-Asp-Trp}^3$  are highlighted in green circle.

which showed that the loop connecting the NTH to TM1 is very flexible [27]. Thus the geometrical constraints of inner wall, together with the mobile NTHs, will be the key determinants of the molecular permeability to larger solutes, including key metabolites and second messengers [28].

Although both models have similar RMSF patterns, there are some differences in the residues that line the pore region including NTH region. At least the first three residues ( $^1\text{Met-Asp-Trp}^3$ ) (Fig. 3) of NTH in high pH state display smaller fluctuations than those in low pH state ( $\sim 1$  Å for former versus  $\sim 3$  Å for latter). In neutral condition, the decreased flexibility of this region is due to Asp2 residues that have direct and occasionally water-bridged hydrogen-bonding interactions with the Met1 (amine group) from neighboring NTHs (details in Section 2.3), resulting in a rigid conformation for the pore region. It is relevant with these three residues of all six protomers that form the constriction in the pore and are expected to modulate the passage of the substrate to the extracellular side. In the acidic state, the interactions between Asp2 and Met1 from neighboring NTH observed in neutral state are interrupted, thus these three residues of NTH undergo large swinging motions (details in section Section 2.3). The differences of RMSF between the neutral and acidic simulations display that the protonation of Asp2 induces a partial destabilizing effect on the NTH, implying that the N-terminal region of connexins can be activated by chemical factor (i.e., pH) and thus participate in the gating of hemichannel.

## 2.2. Cross correlation analysis

To estimate the correlation between the movement of the sub-domains of Cx26 in the neutral and acidic conditions, we have applied cross correlation analysis of the atomic fluctuations for the residues of protein. The correlation coefficients for all possible residue pairs are plotted in Fig. 4, where a value of  $-1$  or  $1$  for a given pair of residues indicates anticorrelated and strongly correlated movement between them respectively, whereas a value of  $0$  indicates no correlation. In this analysis, only correlations larger than  $0.5$  are shown for clarity, positive (in-phase) correlations are colored red (strong) and negative

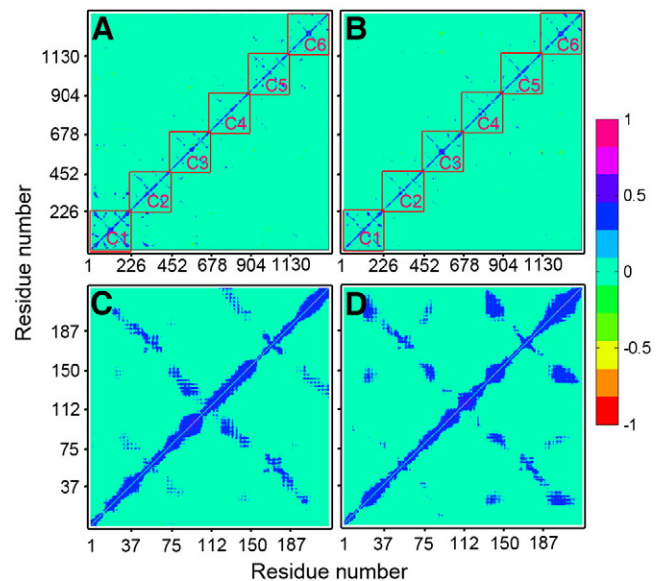


**Fig. 4.** Normalized covariance matrix of the atomic displacements of the C $\alpha$  atoms of Trn1 in different states: (A and C) neutral state, and (B and D) acidic state. Purple regions indicate that the C $\alpha$  atoms move in the same direction (positive correlation), and red regions indicate that they move in opposite directions (negative correlation). Rectangular boxes emanating from main diagonal indicate the location of each segment. For clarity, the blocks corresponding to interactions within one single connexin (C and D) are presented.

(out-of-phase) correlations are colored blue (strong). This allows us to examine interactions within individual connexins and inter-connexin interactions between adjacent proteins, respectively.

In both systems, six segments representing six connexins can be identified by examining the blue spots along the diagonal with off-diagonal blue areas indicating their interconnections. For each segment, the diagonal values of the matrix correspond to autocorrelation, which is extremely unitary, while the off-diagonal elements represent interactions between distinct residues of the same connexin. High positive correlation ( $\sim+0.6$ ) is observed between residues in TM1, TM2, TM3, and TM4, which move in a coupled way. Correlation peaks ( $\sim+0.73$ ) indicate strong interactions among residues Arg32 (TM1) with Gln80 (TM2), Glu147 (TM3), and Ser199 (TM4), Arg143 (TM3) with Asn206 (TM4) and Ser139 (TM3). All these residues are correlated by salt bridge interactions and reside in the TM region. Another important correlation peaks ( $\sim+0.78$ ) present in hydrophobic core around Trp44 which is formed by Ala39 (TM1), Ala40 (TM1), Val43 (E1) and Ile74 (TM2). These intra-protomer interactions maintain during the whole simulations, contributing to tie helices TM1 to TM4 together in both neutral and acidic states.

Interestingly, correlation is decreased by  $\sim 0.2$  by the Pro87 kink of TM2, indicating that Pro87 could decrease the stiffness of the Cx26 protein, therefore the Pro87Leu mutation probably results in a higher stiffness of the Cx26, leading to a reduced capacity of the structure to adjust its inner motions to the external perturbations. This explains why the Pro87Leu mutation links to an aberrant gating [29]. Furthermore, mutations of three residues to proline, i.e., Leu79Pro, Ser85Pro and Leu90Pro, in TM2 are associated with deafness [30]. These mutations probably induce a structural change in TM2, which would affect the cytoplasmic domains including the NTH.

Compared with the high correlation of the amino acids within one segment which moves together, the inter-segment possessing generally lower correlation indicates weaker interactions between adjacent connexins, the largest peak ( $\sim+0.5$ ) is centered on the TM2 (residues 73 to 109), which contacts with the TM1 (residues 21 to 50) and TM4 (residues 185 to 223) of the adjacent connexin. Hence these strong inter-helix coupling motions contribute to tie connexins together. However, the lower degree of correlation ( $\sim+0.3$ ) occurs at NTH, whose bulky side chain is completely exposed to the interior of the connexon, suggesting the uncoupling motions of the interior of the connexon. Thus, the swing of any one of the six NTHs would result in subconductance states of the channel, which accords with the

study that the conformational change of a single protomer is sufficient to initiate channel gating [31].

### 2.3. The closed state of Cx26 in the neutral condition

As a further incentive to investigate the global conformational transition of Cx26, we superpose the initial and final inertial axes of the whole hemichannel (Fig. 5A) and of the connexin (Fig. 5B), respectively. As shown in Fig. 5A, the hemichannel undergoes an overall twist movement where TMD rotates clockwise ( $\sim 4^\circ$ ) and the extracellular domain keeps a relative stable conformation without rotation. While for each connexin, it rotates clockwise around its own axis about  $6^\circ$ . NTHs line the innermost wall of the channel and thus their motions and conformational changes are directly associated with the gating of the Cx26. Upon the propeller twist movement of hemichannel, six Met1 residues show an asymmetric distribution, i.e., three Met1 side chains from C3, C4 and C6 point toward extracellular part of TM2, the rest three point toward cytosol (Fig. 6A). Inspection of the trajectory reveals that C4 and C5 undergo, in advance of other protomers (Fig. 2A), large fluctuations at the cytoplasmic part of the TM2 and TM3 (Figs. 3A and 5A) which would affect the cytoplasmic domains including the NTHs. Thus the NTHs in these protomers protrude into the pore at about 30 ns. The second ensemble of events, which initiates at about 60 ns, mainly affects protomer C3. Meanwhile, NTH of C2 protrudes to the pore in a manner similar to protomers C4 and C5. To better understand these conformational changes, the H-bonding pattern of the residues in NTH is also analyzed since conformational changes are usually associated with alterations in the hydrogen-bonding. When the hemichannel is in the initial conformation (crystal structure), Asp2 establishes hydrogen bonds with the main-chain amide of Thr5 from the adjacent protomer to form a circular girdle, as previously seen in the nicotinic acetylcholine receptor [32]. However, during the MD simulation, these interactions break synchronously (range from 10 ns to 50 ns) due to quaternary reorganization of Cx26 through the rotation of all six protomers over the course of the 100-ns simulations. Alternatively, a more stable hydrogen bond network is eventually established between Asp2 (carboxyl group) and neighboring Met1 (amine group) (Fig. 6A), for example: Asp2(C5) makes hydrogen bonds to Met1(C4) and Met1(C6) respectively, Met1(C3) forms hydrogen bonds to Asp2(C2), and Met1(C5) to Asp2(C4). Occasionally, hydrogen bond between Asp2(C1) and Asp2(C6) is bridged by a water molecule. Once this hydrogen bond network is established, all six NTHs

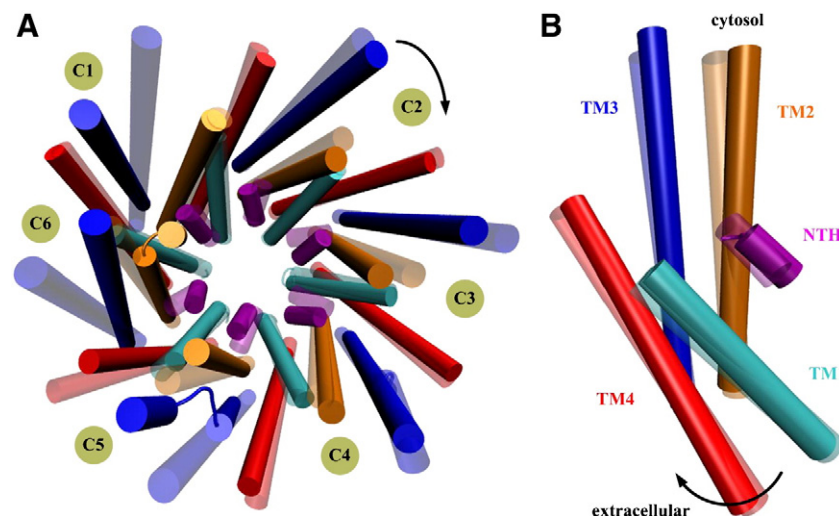


**Fig. 5.** Quaternary changes of Cx26 in neutral state. (A) Top view of the principal axes of inertia for NTH and TMD helices of each protomer (colored in purple, cyan, orange, blue, and red, respectively) at the end of the simulation. The principal axes at the initial simulation are superposed in lighter colors. The number of each protomer is indicated with C1–C6, respectively. (B) A side view of protomer C1.

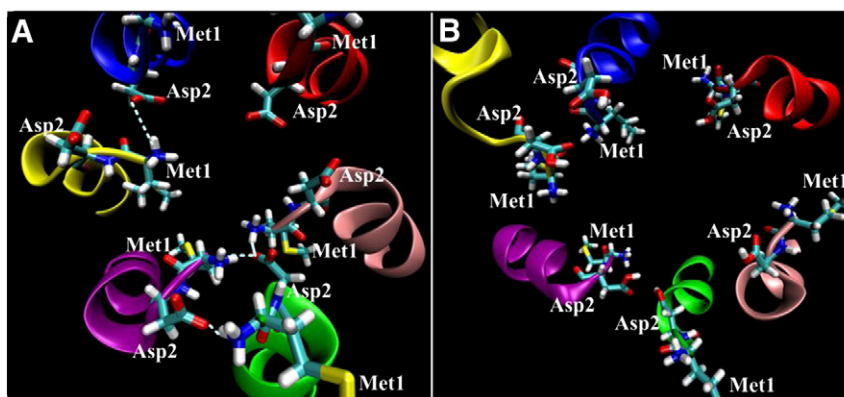


**Fig. 6.** Interactions among six NTHs of Cx26 in (A) neutral state and (B) acidic state. All NTHs are represented as new cartoon, and the color is the same as Fig. 1A. The first two residues in all NTHs are shown in licorice representation, and their atoms are colored as follows: hydrogens in white, carbons in cyan, nitrogen in blue, and oxygens in red, sulfur in yellow.

are bundled together, which protrudes into the pore and substantially closes the channel (Fig. 6A). Combined, these results suggest that the full conformational transition would progress from one protomer to the neighboring one through a “domino-like” process, where a sequence of localized events propagating between neighboring protomers is nested within a global quaternary twist conformational change of the molecule.

To investigate whether the NTH is sufficient to render gating of the hemichannel during these rearrangements, we calculate the pore radius profile averaged over the entire simulation using the “Hole” program [33], this profile provides an overall measure of the pore radius but taking into account dynamic fluctuations in structure (Fig. 7). As for Cx26, the ion permeation pathway consists of the wide extracellular and intracellular vestibules (or entrances), and the narrow transmembrane pore. Considering the conformational fluctuations (represented as error bars) (Fig. 7), the overall shape of both vestibules can be considered constant (about 16 Å in diameter). On the contrary, the transmembrane pore radii decrease prominently during the entire simulation; particularly, the constriction zone at the level

of six Asp2 side chains displays a diameter decreasing from 7 Å (in crystal structure) to about 4 Å (in final conformation) (Fig. 7A). Overall, the simulation on average suggests that the hemichannel Cx26 in neutral pH favors a partially “closed” conformation; in this state the constricted NTH of the pore provides a kinetic barrier to exchange of ions and metabolites between the cytoplasm and the extracellular phase. These results are supported by electron microscopic study of the Cx26 that revealed large densities in the pore at the level of the two membranes, which were interpreted as plugs blocking the hemichannel [19].

#### 2.4. The open state of the Cx26 hemichannel in the acidic condition

For the Cx26’s pH elicited gating, little is known about the precise coupling between the protonation state and the conformational change. The protonation/deprotonation reaction at specific residues is probably rate-limiting and on the ms-to-s time-scale [34]; much slower than the time scales accessible by current MD simulations. Hence, we discard the slow chemical steps of protonation/

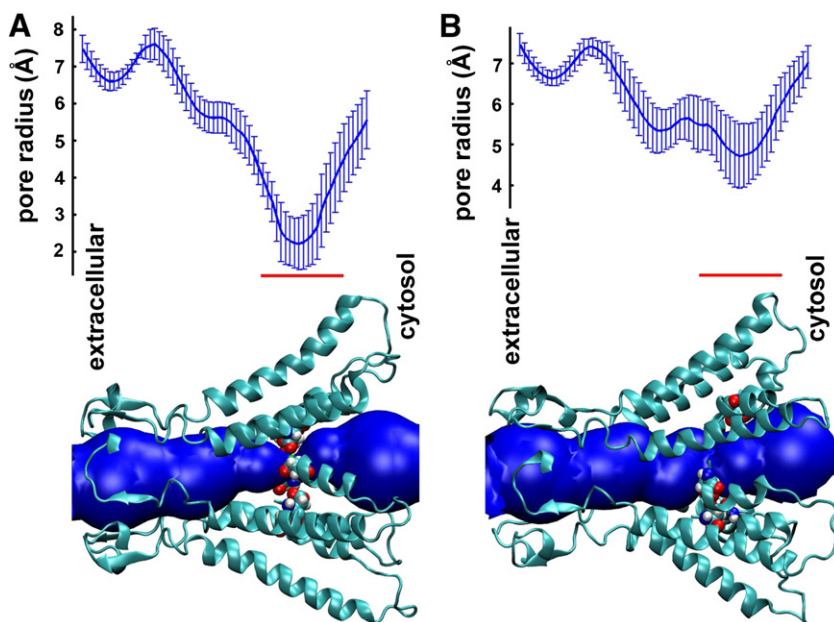


**Fig. 7.** Pore radius. (A) The top panel shows the pore radius along the channel axis for the Cx26 structure (blue) in neutral state. The simulation results are averages over last 70-ns simulation. Standard deviations are shown as error bars. The bottom panel displays side view of Cx26 in neutral pH for the end of the simulation. Asp2 residues facing the pore are depicted in VDW representation. In the side view, only NTH, TM1 and TM2 are shown. The channel pathway is represented as a mesh. (B) pore radius of Cx26 in low pH state.

deprotonation. Here, we artificially perform an instantaneous pH change to compare with the neutral pH, by setting the charge state of the ionizable residues in the channel to their standard state at acidic pH.

In this simulation under the acidic condition, provided that the issue of the precise protonation state of all aspartate and glutamate residues at pH 4.0 is settled, we find that the hemichannel Cx26 displays a twist motion ( $\sim 3^\circ$ ) similar to that in neutral state (Fig. S1). However, the unique behavior of NTH that protrudes into the pore and closes the channel in neutral state disappears. The pore radius profile depicted in Fig. 7B shows that the pore of extracellular and intracellular vestibules have a diameter similar to that of the neutral state of Cx26 (more than 16 Å diameter), whereas diameter of the narrowest pore region around Asp2 widens up to 9.5 Å (in final conformation) relative to the neutral state of Cx26 structure. The value of the pore radius at its narrowest part is even larger than the one observed in the original crystal structure ( $\sim 7$  Å). This result is supported by several recent experimental studies identified that direct hydrogen ion, pH as low as 4 or 5, did not cause channel closure [35–37]. However, different from the effect of direct hydrogen ion,  $\text{CO}_2$  interacts directly with Cx26 probably through the formation of a carbamate on one or more amino groups of lysine residues, or even the N-terminal amino group by a labile covalent bond [38]. Such carbamate formation would alter the charge of these positively charged  $-\text{NH}_3^+$  groups to negatively charged  $-\text{NHCOO}-$  groups [39], thus resulting in the opening of Cx26 gap junctional channels. Interestingly, in our neutral simulation, Asp2 residue is deprotonated and becomes negatively charged, leading to the closure of Cx26 gap junctional channels.

A closer look at the dynamics of the pore in simulation reveals that the protonated Asp2 does not maintain hydrogen bonds with Met1 from adjacent protomer (Fig. 6B), releasing the restraints of six NTHs. The Met1–Asp2 residues from one protomer pointing to the neighboring NTHs form a circular girdle, maintaining the pore in the open conformation (Fig. 7B). Together with the results in neutral state, this suggests that the concerted conformational changes of NTH (particular for protonation/deprotonation of the Asp2) are required for the successful passage of water and ions or metabolites through the hemichannel. Furthermore, it is worth noting that the widening pore of Cx26 in acidic state is still narrower than that of Cx32 which ranges from, 1.1 nm estimated by perfusion of polyethylene glycol probes [39] to, 1.5 nm estimated [40] based on cryoelectron microscopy data [41]. This is supported by the limiting pore width of connexin channels that is directly assessed by using sets of highly homologous uncharged molecules [42]. To understand what

will happen if the pH is increased to a higher value, we performed one additional 70-ns simulation at pH 6.0, in which all Asp2 residues become deprotonated and all His100 at extracellular of TM2 are protonated. We observed a similar pore radius distribution to that under neutral state (Fig. S2), confirming that the deprotonated Asp2 will constrict the pore.

Given the structure with a widened pore size in acidic state and with a narrowed one in neutral state, it is of interest to examine whether these conformations are capable of ion permeation. Rather than conducting ion-pulling simulations [43], we directly observe ionic conduction in normal MD simulations. The results show that, on a 100-ns timescale, 8  $\text{Cl}^-$  ion permeation events take place in acidic state and 2 in neutral state. i.e., we can obtain the passage (or flow) rates of  $\text{Cl}^-$  in acidic state 4 times over those in neutral state. From this result one can see that  $\text{Cl}^-$  ion can enter the pore in neutral state with more difficulty than they do in acidic state. This low anion permeation in neutral state probably arises from two aspects: 1) the pore around Asp2 region favors a closed conformation in this condition (Fig. 6A), presenting a kinetic barrier to the entry of water and ions into the channel from the cytosol; 2) the six Asp2, each with a negative charge (deprotonation) in this state, are incorporated as a negative potential at the channel entrance (Fig. 6A), preventing  $\text{Cl}^-$  being accessible to the channel. While in acidic state, these kinetic and potential barriers are relieved due to the protonation of Asp2, thereby increasing the conductivity of anion. In summary, the conductivity of anion of Cx26 is sensitive to the protonation state of Asp2 inside the pore.

It is noteworthy that our predicted model that is permeable to anions ( $\text{Cl}^-$ ) but not to cations ( $\text{Na}^+$ ) in neutral simulation is consistent with the very recent study by Kwon et al. [44]. Both studies are inconsistent with the experimental results that the Cx26 appears to be permeable to both cationic and anionic tracers [45,46]. The difference in permeability to  $\text{Cl}^-$  and  $\text{Na}^+$  is probably accounted for the fact that the protein is being posttranslationally modified within cells by lysine or Met-1 acetylation [44]. Closer inspection reveals that anions are attracted by the channel and bind close to the side chain of Lys41, which locates at the TM1/E1 boundary that has been suggested to be involved in voltage sensing [17]. The direct interaction between Lys41 residues and  $\text{Cl}^-$  (about 10 ns) indicates that the lysine in each protomer probably serves as the selectivity filter or just a binding site for anions (Fig. 8).

Earlier simulations suggested that the water density in the pore can also be used as an indicator of the conductance state of the channel [26]. The time-averaged water density from both the acidic and neutral simulations is shown in Fig. 9. The simulation under acidic

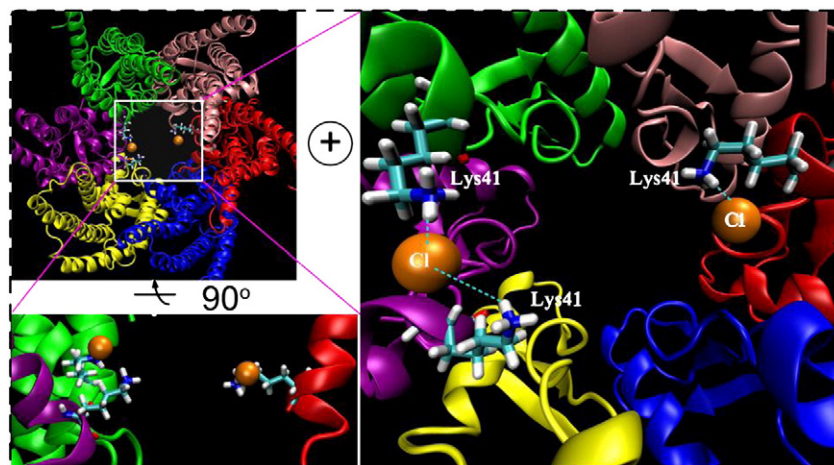


**Fig. 8.** Chloride ions bind close to the side chain of lys41. The top left picture is the top view of the whole structure of Cx26. Lys41 residues from C1, C4 and C5 are presented as licorice, two chloride ions are shown as brown spheres. The bottom left is the side view of the chloride ions and lys41 residues. The right picture is the enlargement for the structure of two chloride ions and three lys41.

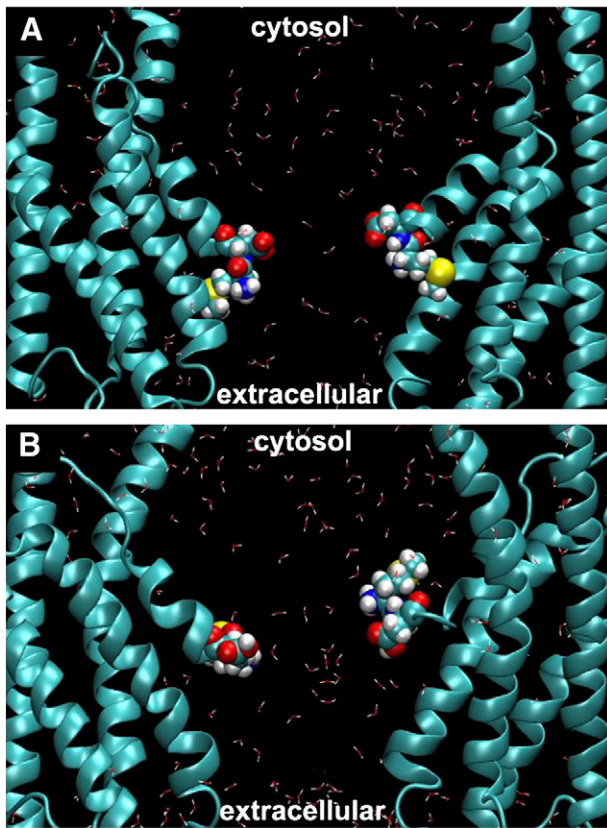


**Fig. 9.** The Time-Averaged Water Density in the hemichannel. (A) During the neutral simulation. (B) During the acidic simulation commencing from the final TMD conformer. Six NTHs are shown in new cartoons. Residues Met1–Asp2 are shown in VDW representation. All observed water positions during a 20-ns interval are depicted as lines.

condition results in a higher water occupancy than in the neutral simulation. Furthermore, the water density volume displays a sharp constriction for water passage near NTH in both simulations. However, closer inspection of the trajectories reveals that the side chain orientations as well as the backbone conformations of Asp2 are different in the two simulations. In neutral simulation, the flow of water into the channel is restricted at this region, and only 8 water molecules pass this narrow pore region during the last 10 ns of the simulation. Whereas in acidic simulation, the expansion of this pore region facilitates the water molecules pass through the gate (15 water molecules during the last 10 ns of the simulation), suggesting that the constriction in neutral state has been partially removed by deprotonated Asp2 in acidic state. This observation confirms that the simulation samples an open state in acidic state,

with a large and continuous water column enabling permeation of ions across the channel.

### 2.5. Implications for the mechanism of proton conduction

As mentioned in the **Introduction** section, the hemichannels can control an exchange of ions and metabolites between the cytoplasm and extracellular milieu and thus influence the spatial dissipation of intercellular ions and metabolites. Although it has been proposed that this modulation arises from direct protonation of connexin [47], locating the channel gate(s) in hemichannel is still a challenging task, because experiments on mutation of histidine or methionine suggest a location at either the intracellular [11,12] or the transmembrane domain of hemichannel [9]. To address this, we compare the pore radius profiles of Cx26 in the neutral and the acidic states. The overall shape of the pore profiles for both states of Cx26 reveals a significant barrier at the NTH of the channel, particularly for Asp2 residue, suggesting a putative channel ‘gate’ (Fig. 7). Since the Asp2 residue in the Cx26 structure might function as a channel gate, we conduct another 70-ns simulation of Cx26 with all Asp2 mutated into Ala2 to further characterize whether mutation in Asp2 can alter the gating of the channel. We find that these mutations disrupt the original hydrogen bond network established between Asp2 and neighboring Met1, resulting in that the mutant channel has obviously larger pore radius of the constriction zone than those of wild type Cx26 protein (see supporting Fig. S3). These data indicate that the Asp2Ala mutations in Cx26 may have higher junctional conductances of mutant channels than those of their wild type counterparts, confirming the crucial role of Asp2 residues for the control of channel activity. Combined, the most important mechanistic insights gained from these simulations are that Cx26 has two different configurations: 1) the neutral state of Cx26 has a small, tightly closed pore around NTH region (average RMSF = ~1 Å), particularly, this pore is clamped shut by interhelical interactions involving for Asp2; 2) the acidic state of Cx26 has a large, flexibly opening pore around NTH region (average RMSF = ~3 Å).

Having established that the protonation of Asp2 can induce the channel conformation changes, it is interesting to infer the possible conductance mechanism by which gap junction channel regulates the transfer of various solutes, such as second messenger. Based on the simulation results, in addition to the physiological fact that pH < 6.50 can induce electrical and biochemical uncoupling between cells [48], Fig. 10 schematically outlines a model for the ion or metabolite conduction mediated by hemichannel. When one cell has a normal pH value of ~7.2, the hemichannel in the membrane has a closed conformation which obstructs the exchange of ions or metabolites. However, when acid generation localized in this cell, Asp2 in the hemichannel exposed to the cytoplasm can be easily protonated,

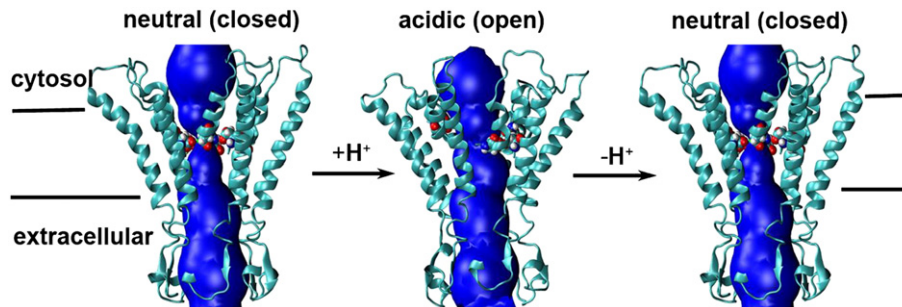


**Fig. 10.** A proposed mechanism of  $H^+$  transport cycle. The hemichannel in the membrane has a closed conformation in neutral state, which obstructs the exchange of ions. When acid generation localized in the cell, Asp2 in the NTH exposed to the cytoplasm can be easily protonated, thus leading to the opening of the pore around NTH, this opening conformation facilitates the flow of a proton to easily pass through the hemichannel into extracellular space. As much as  $H^+$  ion transmission occurs, the cytoplasmic region becomes more alkaline. The increase of pH to normal physiological values makes the hemichannel revert to its initial closed conformation, which stops the  $H^+$  transmission until eventually equilibrium is reached.

thus leading to the opening of the pore around NTH, this opening conformation of the hemichannel facilitates the flow of an ion or metabolite to easily pass through the hemichannel into extracellular space, thereby providing a mechanism for spatially regulating ion or metabolites. Since gating is a reversible process and alkalization rather than acidification reduces the junctional conductance of Cx26 hemichannels, the increase of pH to normal physiological values makes the hemichannel revert to its initial closed conformation, which stops the ion transmission until eventually equilibrium is reached. This model provides a preliminary conduction cycle of hemichannel, suggesting that the pH sensitivity of hemichannel permeability is a sophisticated mechanism for regulating cell signaling molecules, though more complex mechanisms involving cycling between protonation states with a net difference of a single proton are possible.

Intercellular signaling is one of the most essential properties of multi-cellular organisms. Gap junctions contain hundreds of cellular communication channels that allow the passage of molecules including ions and metabolites, nucleotides and small peptides.  $H^+$  activation of junctional permeability may link increased ion activity to improved cell coupling, the better to meet mechanical demand. Notably, in normal cells, Cx26 channels close in response to acidification due to the effects of taurine or some other naturally occurring cytoplasmic aminosulfonate. So the effect of protonation of Asp2 that leads to an increase in the size of the pore will probably be masked by the effects of cytoplasmic aminosulfonates. However, neutralization of the negative charge of Asp2 will probably occur in some disease condition, which opens gap-junctional hemichannels. Therefore, mutation of residue Asp3 in either Cx43 [49] or Cx46 [50] (have a similar location to Asp2 in Cx26) probably has decreased conductance due to a severely reduced open probability, potentially explaining autosomal dominant inheritance of the disease [51,52]. Furthermore,  $H^+$  activation benefits for explaining that hypoxia and simulated ischemia can open gap-junctional hemichannels in neurons [51] and cardiac myocytes [52], as these conditions motivate a decrease of  $pH_i$ . Here, we do not exclude the existence of the other gating mechanisms in hemichannel, because connexins are thought to use several gating mechanisms such as the transjunctional voltage gating and loop gating [11]. In addition that the Asp2 residue functions as a chemical gate in this study, this residue has also been suggested as an electrostatic gate [9], which is perhaps unique to the Cx26 gap junction channel.

### 3. Conclusion

The present work provides a possible atomistic model of the gating process for the human Cx26 gap junction channel, in which the NTH has the main role in sensing pH within the conductive pore and in forming the plug to close the pore. In neutral state, six NTHs distribute asymmetrically and they (C1 to C6) gather together through H-bonding networks, strongly suggesting that the cluster of the four NTHs can block the pore of Cx26 (less than 4 Å diameter). This process occurs very rapidly with an initial closure event on the 40 ns time scale. While in the acidic state, the protonation of the pore-lining residues Asp2 could potentially drive a conformational change that enables the Met1–Asp2 to lock in an “open” orientation while facing the hydrophilic pore (more than 9 Å diameter). This conformational change allows the channel to have a close-to-open transition, thereby providing a channel gating mechanism for the protein controlling ion permeation which is sensitive to the protonation state of Asp2 inside the pore. Furthermore, these structural and mechanistic insights may aid the design of new experiments relevant for elucidating the structure/function relationships in gap junction channels. It also probably guide the devise of novel mutants with impaired conducting as a tool for selectively knocking down or knocking out connexin function.

## 4. Materials and methods

### 4.1. Model preparation

In the most recent crystal structure of Cx26 (PDB code 2ZW3 at 3.5 Å resolution) [9], the whole structure of each protomer—except for residues 1, 110–124 and 218–226 that correspond to most of the cytoplasmic loop and the carboxy-terminal segment, respectively—was success fully modeled in electron density maps. In the present work, initially, we added a single Met to the N-terminus assuming  $\alpha$ -helical backbone torsion angles. Then, the missing TM2–TM3 loop is reconstructed using the loop-building algorithm implemented in the Biopolymer module in Sybyl 6.9 package (Tripos Associates, St. Louis, MO). We have selected the loop structure with the lowest predicted energy. Thirdly, the missing C-terminal segment of TM4 is assumed to adopt an  $\alpha$ -helical structure. Finally, the missing hydrogen atoms, and side chains in the crystal structure (Fig. 1, the cartoon highlighted in red) were reconstructed in stereochemically preferred conformations. In order to assign standard protonated states for pH 4.0 to all acidic side chains, we calculate the pKa for Cx26 by using the program H++ [53], in which the calculations are based on the standard continuum solvent methodology [54], within the frameworks of either the generalized Born (GB) or the Poisson–Boltzmann (PB) models. It has to be emphasized that this protonation state at pH 4.0 should be considered as a working hypothesis but is in no way a resolved issue. We are still unsure about the right protonation state at acidic pH and this problem requires refined methods to predict side-chain pKas for membrane proteins in their native environment [24]. Then Cx26 protein was embedded into a fully equilibrated palmitoyloleoylphosphatidylcholine (POPC) lipid bilayer. The final simulation system consisted of 500 POPC molecules, 102,330 SPCE water molecules and 397  $Na^+$  and 451  $Cl^-$  (pH 4.0)/486  $Cl^-$  (pH 4.0). In both simulations, the net charge of the system was neutralized with counterions, achieving a salt concentration of 0.15 M.

### 4.2. Molecular dynamic simulations

Molecular dynamics simulations were carried out using the GRO-MACS 4.0 MD package [55] applying periodic boundary conditions. The protein and lipids were represented using the CHARMM27 force field [56] with CMAP corrections [57], whereas water was described with the SPCE model [58]. The bond lengths were constrained using the LINCS [59]. Short-range non-bonded interactions were calculated using a cutoff distance of 10 Å, and long-range electrostatic interactions were calculated using the particle mesh Ewald (PME) method [60]. The integration time-step was set at 2 fs. For all simulations, the temperature was set at 300 K with Berendsen coupling [61]. The pressure was controlled by the Berendsen barostat at 1 atm with the independent (semiisotropic) coupling in the xy and z directions.

### 4.3. Cross-correlation analyses

In the present analysis, the extent of correlated motions between residues is represented by the magnitude of the corresponding correlation coefficient between their  $C\alpha$  atoms. The cross correlation matrix ( $C_{ij}$ ) of the atomic displacements of atoms  $i$  and  $j$  is given by:

$$C_{ij} = \frac{(\mathbf{r}_i - \bar{\mathbf{r}}_i)(\mathbf{r}_j - \bar{\mathbf{r}}_j)}{\sqrt{(\mathbf{r}_i - \bar{\mathbf{r}}_i)^2(\mathbf{r}_j - \bar{\mathbf{r}}_j)^2}},$$

where  $\mathbf{r}_i$  and  $\mathbf{r}_j$  are the positions and  $\bar{\mathbf{r}}_i$  and  $\bar{\mathbf{r}}_j$  are the mean positions of atoms  $i$  and  $j$ . The angle brackets denote an ensemble average. The cross correlation was calculated as block average over time from 30 to 100 ns from the MD trajectory. Positively correlated residues

move in the same direction, while (negatively) anti-correlated residues move in the opposite direction.

## Acknowledgements

This work is supported by the high-performance computing platform of Northwest A & F University, and is financially supported by the National Natural Science Foundation of China (Grant No. 31170796), the Fund of Northwest A & F University and also the Scholarship Award for Excellent Doctoral Student granted by the Ministry of Education.

## Appendix A. Supplementary data

Supplementary data to this article can be found online at doi:10.1016/j.bbammem.2011.12.027.

## References

- [1] V. Lyall, T.U. Biber, Potential-induced changes in intracellular pH, *Am. J. Physiol.* 266 (1994) 685–696.
- [2] A. Diarra, C. Sheldon, C.L. Brett, K.G. Baimbridge, J. Church, Anoxia-evoked intracellular pH and  $\text{Ca}^{2+}$  concentration changes in cultured postnatal rat hippocampal neurons, *Neuroscience* 93 (1999) 1003–1016.
- [3] J.A. Madden, P.A. Keller, J.G. Kleinman, Changes in smooth muscle cell pH during hypoxic pulmonary vasoconstriction: a possible role for ion transporters, *Physiol. Res.* 49 (2000) 561–566.
- [4] J.C. Sáez, M.A. Retamal, D. Basilio, F.F. Bukauskas, M.V.L. Bennett, Connexin-based gap junction hemichannels: gating mechanisms, *Biochim. Biophys. Acta Biomembr.* 1711 (2005) 215–224.
- [5] M. Yeager, B.J. Nicholson, Structure of gap junction intercellular channels, *Curr. Opin. Struct. Biol.* 6 (1996) 183–192.
- [6] A.L. Harris, Emerging issues of connexin channels: biophysics fills the gap, *Q. Rev. Biophys.* 34 (2001) 325–472.
- [7] N.M. Kumar, N.B. Gilula, The gap junction communication channel, *Cell* 84 (1996) 381–388.
- [8] J. Eiberger, J. Degen, A. Romualdi, U. Deutsch, K. Willecke, G. Söhl, Connexin genes in the mouse and human genome, *Cell Commun. Adhes.* 8 (2001) 163–165.
- [9] S. Maeda, S. Nakagawa, M. Suga, E. Yamashita, A. Oshima, Y. Fujiyoshi, T. Tsukihara, Structure of the connexin 26 gap junction channel at 3.5 Å resolution, *Nature* 458 (2009) 597–602.
- [10] M. Delmar, W. Coombs, P. Sorgen, H.S. Duffy, S.M. Taffet, Structural bases for the chemical regulation of connexin43 channels, *Cardiovasc. Res.* 62 (2004) 268–275.
- [11] C. Peracchia, Chemical gating of gap junction channels; roles of calcium, pH and calmodulin, *Biochim. Biophys. Acta Biomembr.* 1662 (2004) 61–80.
- [12] B.J. Hirst-Jensen, P. Sahoo, F. Kieken, M. Delmar, P.L. Sorgen, Characterization of the pH-dependent interaction between the gap junction protein connexin43 carboxyl terminus and cytoplasmic loop domains, *J. Biol. Chem.* 282 (2007) 5801–5813.
- [13] J.F. Ek, M. Delmar, R. Perzova, S.M. Taffet, Role of histidine 95 on pH gating of the cardiac gap junction protein connexin43, *Circ. Res.* 74 (1994) 1058–1064.
- [14] X.G. Wang, C. Peracchia, Positive charges of the initial C-terminus domain of Cx32 inhibit gap junction gating sensitivity to  $\text{CO}_2$ , *Biophys. J.* 73 (1997) 798–806.
- [15] H.S. Duffy, A.W. Ashton, P. O'Donnell, W. Coombs, S.M. Taffet, M. Delmar, D.C. Spray, Regulation of connexin43 protein complexes by intracellular acidification, *Circ. Res.* 94 (2004) 215–222.
- [16] E.C. Beyer, G.M. Lipkind, J.W. Kyle, V.M. Berthoud, Structural organization of intercellular channels II. Amino terminal domain of the connexins: sequence, functional roles, and structure, *Biochim. Biophys. Acta Biomembr.* (in press).
- [17] V.K. Verselis, C.S. Ginter, T.A. Bargiello, Opposite voltage gating polarities of two closely related connexins, *Nature* 368 (1994) 348–351.
- [18] L. Ebihara, V.M. Berthoud, E.C. Beyer, Distinct behavior of connexin56 and connexin46 gap junctional channels can be predicted from the behavior of their hemi-gap-junctional channels, *Biophys. J.* 68 (1995) 1796–1803.
- [19] A. Oshima, K. Tani, Y. Hiroaki, Y. Fujiyoshi, G.E. Sosinsky, Three-dimensional structure of a human connexin26 gap junction channel reveals a plug in the vestibule, *Proc. Natl. Acad. Sci. USA* 104 (2007) 10034–10039.
- [20] A. Oshima, K. Tani, Y. Hiroaki, Y. Fujiyoshi, G.E. Sosinsky, Projection structure of a N-terminal deletion mutant of connexin 26 channel with decreased central pore density, *Cell Commun. Adhes.* 15 (2008) 85–93.
- [21] G. Khelashvili, A. Grossfeld, S.E. Feller, M.C. Pitman, H. Weinstein, Structural and dynamic effects of cholesterol at preferred sites of interaction with rhodopsin identified from microsecond length molecular dynamics simulations, *Proteins* 76 (2009) 403–417.
- [22] R.O. Dror, D.H. Arlow, D.W. Borhani, M.Ø. Jensen, S. Piana, D.E. Shaw, Identification of two distinct inactive conformations of the beta2-adrenergic receptor reconciles structural and biochemical observations, *Proc. Natl. Acad. Sci. USA* 106 (2009) 4689–4694.
- [23] P. Bjelkmar, P.S. Niemelä, I. Vattulainen, E. Lindahl, Conformational changes and slow dynamics through microsecond polarized atomistic molecular simulation of an integral Kv1.2 ion channel, *PLoS Comput. Biol.* 5 (2) (2009) e1000289.
- [24] H. Nury, F. Poitevin, C. Van Renterghem, J.P. Changeux, P.J. Corringer, M. Delarue, M. Baaden, One-microsecond molecular dynamics simulation of channel gating in a nicotinic receptor homologue, *Proc. Natl. Acad. Sci. USA* 107 (2010) 6275–6280.
- [25] J.D. Faraldo-Gómez, L.R. Forrest, M. Baaden, P.J. Bond, C. Domene, G. Patargias, J. Cuthbertson, M.S.P. Sansom, Conformational sampling and dynamics of membrane proteins from 10-nanosecond computer simulations, *Proteins* 57 (2004) 783–791.
- [26] M. Baaden, M.S. Sansom, OMPT: molecular dynamics simulations of an outer membrane enzyme, *Biophys. J.* 87 (2004) 2942–2953.
- [27] P.E. Purnick, D.C. Benjamin, V.K. Verselis, T.A. Bargiello, T.L. Dowd, Structure of the amino terminus of a gap junction protein, *Arch. Biochem. Biophys.* 381 (2000) 181–190.
- [28] V.H. Hernandez, M. Bortolozzi, V. Pertegato, M. Beltramello, M. Giarin, M. Zaccolo, S. Pantano, F. Mammano, Unitary permeability of gap junction channels to second messengers measured by FRET microscopy, *Nat. Methods* 4 (2007) 353–358.
- [29] T.M. Suchyna, L.X. Xu, F. Gao, C.R. Fournier, B.J. Nicholson, Identification of a proline residue as a transduction element involved in voltage gating of gap junctions, *Nature* 365 (1993) 847–849.
- [30] D.W. Laird, Life cycle of connexins in health and disease, *Biochem. J.* 394 (2006) 527–543.
- [31] S. Oh, C.K. Abrams, V.K. Verselis, T.A. Bargiello, Stoichiometry of transjunctional voltage-gating polarity reversal by a negative charge substitution in the amino terminus of a connexin 32 chimera, *J. Gen. Physiol.* 116 (2000) 13–31.
- [32] A. Miyazawa, Y. Fujiyoshi, N. Unwin, Structure and gating mechanism of the acetylcholine receptor pore, *Nature* 423 (2003) 949–955.
- [33] O.S. Smart, J.C. Neduveilil, X. Wang, B.A. Wallace, M.S. Sansom, HOLE: a program for the analysis of the pore dimensions of ion channel structural models, *J. Mol. Graph.* 14 (1996) 354–360.
- [34] L.H. Pinto, R.A. Lamb, Influenza virus proton channels, *Photochem. Photobiol. Sci.* 5 (2006) 629–632.
- [35] D. Locke, F. Kieken, L. Tao, P.L. Sorgen, A.L. Harris, Mechanism for modulation of gating of connexin26-containing channels by taurine, *J. Gen. Physiol.* 138 (2011) 321–339.
- [36] M.V.L. Bennett, Not what you thought: How  $\text{H}^+$  ions combine with taurine or other aminosulfonates to close Cx26 channels, *J. Gen. Physiol.* 138 (2011) 377–380.
- [37] C.G. Bevans, A.L. Harris, Regulation of connexin channels by pH. Direct action of the protonated form of taurine and other aminosulfonates, *J. Biol. Chem.* 274 (1999) 3711–3719.
- [38] R.T. Huckstepp, R. Eason, A. Sachdev, N. Dale,  $\text{CO}_2$ -dependent opening of connexin 26 and related  $\beta$  connexins, *J. Physiol.* 588 (2010) 3921–3931.
- [39] X.Q. Gong, B.J. Nicholson, Size selectivity between gap junction channels composed of different connexins, *Cell Commun. Adhes.* 8 (2001) 187–192.
- [40] G.E. Sosinsky, B.J. Nicholson, Structural organization of gap junction channels, *Biochim. Biophys. Acta Biomembr.* 1711 (2005) 99–125.
- [41] V.M. Unger, N.M. Kumar, N.B. Gilula, M. Yeager, Three-dimensional structure of a recombinant gap junction membrane channel, *Science* 283 (1999) 1176–1180.
- [42] A.L. Harris, Connexin channel permeability to cytoplasmic molecules, *Prog. Biophys. Mol. Biol.* 94 (2007) 120–143.
- [43] T.W. Allen, O.S. Andersen, B. Roux, Energetics of ion conduction through the gramicidin channel, *Proc. Natl. Acad. Sci. USA* 101 (2004) 117–122.
- [44] T. Kwon, A.L. Harris, A. Rossi, T.A. Bargiello, Molecular dynamics simulations of the Cx26 hemichannel: evaluation of structural models with Brownian dynamics, *J. Gen. Physiol.* 138 (2011) 475–493.
- [45] F.L. Cao, R. Eckert, C. Elfgang, J.M. Nitsche, S.A. Snyder, D.F. Hulser, K. Willecke, B.J. Nicholson, A quantitative analysis of connexin-specific permeability differences of gap junctions expressed in HeLa transfectants and *Xenopus* oocytes, *J. Cell Sci.* 111 (1998) 31–43.
- [46] M. Beltramello, M. Bicego, V. Piazza, C.D. Ciubotaru, F. Mammano, P. D'Andrea, Permeability and gating properties of human connexins 26 and 30 expressed in HeLa cells, *Biochem. Biophys. Res. Commun.* 305 (2003) 1024–1033.
- [47] D.C. Spray, A.L. Harris, M.V.L. Bennett, Voltage dependence on junctional conductance in early amphibian embryos, *Science* 204 (1979) 432–434.
- [48] M. Zaniboni, A. Rossini, P. Swietach, N. Banger, K.W. Spitzer, D. Richard, Vaughan-Jones proton permeation through the myocardial gap junction, *Circ. Res.* 93 (2003) 726–735.
- [49] W.A. Paznekas, B. Karczeski, S. Vermeer, R.B. Lowry, M. Delatycki, F. Laurence, P.A. Koivisto, L. Van Maldergem, S.A. Boyadjev, J.N. Bodurtha, J.E. Wang, *GJA1* mutations, variants, and connexin 43 dysfunction as it relates to the oculodentodigital dysplasia phenotype, *Hum. Mutat.* 30 (2009) 724–733.
- [50] P.K. Addison, V. Berry, K.R. Holden, D. Espinal, B. Rivera, H. Su, A.K. Srivastava, S.S. Bhattacharya, A novel mutation in the connexin 46 gene (*GJA3*) causes autosomal dominant zonular pulverulent cataract in a Hispanic family, *Mol. Vis.* 12 (2006) 791–795.
- [51] R.J. Thompson, N. Zhou, B.A. MacVicar, Ischemia opens neuronal gap junction hemichannels, *Science* 312 (2006) 924–927.
- [52] S.A. John, R. Kondo, S.Y. Wang, J.I. Goldhaber, J.N. Weiss, Connexin-43 hemichannels opened by metabolic inhibition, *J. Biol. Chem.* 274 (1999) 236–240.
- [53] J.C. Gordon, J.B. Myers, T. Folta, V. Shoja, L.S. Heath, A. Onufriev,  $\text{H}^+ + :$  a server for estimating pKas and adding missing hydrogens to macromolecules, *Nucleic Acids Res.* 33 (2005) 368–371.
- [54] D. Bashford, M. Karplus, pKa's of ionizable groups in proteins: atomic detail from a continuum electrostatic model, *Biochemistry* 29 (1990) 10219–10225.
- [55] B. Hess, C. Kutzner, D. Van Der Spoel, E. Lindahl, GROMACS 4: algorithms for highly efficient, load-balanced, and scalable molecular simulation, *J. Chem. Theory Comput.* 4 (2008) 435–447.
- [56] A.D. MacKerell, D. Bashford, M. Bellott, R.L. Dunbrack, J.D. Evanseck, M.J. Field, S. Fischer, J. Gao, H. Guo, S. Ha, D. JosephMcCarthy, L. Kucunir, K. Kuczera,

- F.T.K. Lau, C. Mattos, S. Michnick, T. Ngo, D.T. Nguyen, B. Prohom, W.E. Reiher, B. Roux, M. Schlenkrich, J.C. Smith, R. Stote, J. Straub, M.W. Tanabe, J. WioorkiewiczKuczera, D. Yin, M. Karplus, All-atom empirical potential for molecular modeling and dynamics studies of proteins, *J. Phys. Chem. B* 102 (1998) 3586–3617.
- [57] A.D. MacKerell, M. Feig, C.L. Brooks III, Extending the treatment of backbone energetics in protein force fields: limitations of gas-phase quantum mechanics in reproducing protein conformational distributions in molecular dynamics simulations, *J. Comput. Chem.* 25 (2004) 1400–1415.
- [58] H.J.C. Berendsen, J.R. Grigera, T.P. Straatsma, The missing term in effective pair potentials, *J. Phys. Chem.* 91 (1987) 6269–6271.
- [59] B. Hess, H. Bekker, H.J.C. Berendsen, J. Fraaije, LINCS: a linear constraint solver for molecular simulations, *J. Comput. Chem.* 18 (1997) 1463–1472.
- [60] T. Darden, D. York, L. Pedersen, Particle mesh Ewald. An  $N \cdot \log(N)$  method for Ewald sums in large systems, *J. Chem. Phys.* 98 (1993) 10089–10092.
- [61] H.J.C. Berendsen, J.P.M. Postma, W.F. van Gunsteren, A. DiNola, J.R. Haak, Molecular dynamics with coupling to an external bath, *J. Chem. Phys.* 81 (1984) 3684–3690.